JOURNAL OF PROPULSION AND POWER
Vol. 10, No. 3, May–June 1994

Vane-Blade Interaction in a Transonic Turbine, Part I: Aerodynamics

K. V. Rao* and R. A. Delaney†
Allison Gas Turbine Division, Indianapolis, Indiana 46206
and
M. G. Dunn‡
Calspan Advanced Technology Center, Buffalo, New York 14225

Part I of this article presents results of a computational investigation of the effects of blade row interaction on the aerodynamics of a transonic turbine stage. The predictions are obtained using a two-dimensional unsteady Navier-Stokes code based on an explicit Runge-Kutta algorithm and an overlapping O-H grid system. This code simulates the flow in time-accurate fashion using nonreflective stage inflow and outflow boundary conditions and phase-lagging procedures for modeling arbitrary airfoil counts in the vane and blade rows. The O-H grid provides high spatial resolution of the high gradient regions near the airfoil surfaces and allows for arbitrary placement of stage inflow and outflow boundaries. Unsteady and time-averaged airfoil surface pressure predictions are compared with those from an older version of the code based on the explicit hopscotch algorithm and an O-grid system, and experimental data obtained in a short-duration shock tunnel facility.

Introduction

MOST of the performance improvements in modern axial turbines can be attributed to the extensive use of advanced computational fluid dynamics (CFD) codes in the design process. Today, highly accurate CFD codes are used routinely to optimize flow path and blading contours. For the most part, these codes were developed for steady flow through isolated blade rows and do not account for the unsteady potential, wake, and shock wave interactions between neighboring blade rows.

Considerable research has been performed to determine the effect of unsteady interactions on turbine aerodynamics. Hunter[1] and Dring et al.[2] performed large-scale, low-speed turbine rig tests and investigated the effect of varying the spacing between the vane and blade rows. They detected considerable differences between the rotor exit conditions for the different vane-blade spacings which were attributed to unsteady phenomena. Scholz[3] and Sharma et al.[4] determined that blade-element losses in the unsteady stage environment are larger than those in a steady cascade. They estimated that the additional losses induced by unsteady effects may be on the order of 25–100% of the losses for airfoils in a steady cascade.

The finding of increased loss for unsteady interactive flows is also supported by fundamental studies of the effect of stator wakes on the downstream rotor boundary-layer transition performed by Pfeil et al.,[5] Paxson and Mayle,[6] and Addison and Hodson.[7,8] These studies have shown that unsteadiness created by the vane wakes has significant effects on the boundary-layer behavior for transitional laminar-turbulent flows. For these flows, the laminar-turbulent transition location and profile losses are affected by the periodic unsteadiness created by the upstream wakes.

For transonic turbines, significant unsteadiness occurs due to vane trailing-edge shocks impinging on the downstream rotor blades. Early work on the study of the effect of the vane trailing-edge shocks on the rotor flowfield was conducted by Doorly and Oldfield[9] in a linear cascade with upstream rotating wires generating shocks that simulated vane trailing-edge shocks. They found that the shock was a major source of unsteadiness in the downstream blade row. In a computational study, Giles[10] found that vane trailing-edge shocks produced a 40% lift variation on the rotor airfoils. Investigations into vane-blade interactions in a full-scale transonic turbine have been reported by Lewis et al.[11] and Dunn et al.[12] Time-averaged data from these investigations showed reduced loading on the vane, and negative incidence on the downstream blade resulting from the shock wave-rotor interaction. Other computational and experimental investigations of blade row interactions in transonic turbines have been reported by Ashworth,[13] Guenette et al.,[14] and Rangwalla et al.[15] All of these investigations have shown strong effects of shock waves on the unsteady vane-blade interactive flow.

This two-part article presents results of a computational/experimental investigation of the effects of vane-blade interaction on aerodynamics and heat transfer in a transonic turbine stage. In Part I of the article, a brief description of the experimental facility/instrumentation is given. An embedded O-H grid scheme for predicting the unsteady flow in a turbine stage is presented, and aerodynamic results are compared with experimental measurements previously taken in a short-duration shock tunnel facility. Part II of the article presents comparisons of predicted and measured airfoil surface heat transfer rates on the vane and blade. The comparisons are made on the basis of both phase-resolved and time-averaged data.

Experimental Apparatus

The experiments were performed in a short duration shock tunnel. This tunnel consists of an 18.5-in.-i.d. shock tube with 40-ft-long driver tube, 60-ft-long driven tube, a primary nozzle, and a 9-ft-diam, 34-ft-long dump tank. The test gas used in these experiments was air. The facility can accommodate the physical size and weight flow requirements of large tur-

Received Jan. 19, 1992; presented as Paper 92-3323 at the AIAA/SAE/ASME/ASEE 28th Joint Propulsion Conference, Nashville, TN, July 6–8, 1992; revision received Aug. 25, 1993; accepted for publication Aug. 26, 1993.

*Senior Project Engineer, Advanced Turbomachinery Department, P.O. Box 420. Member AIAA.
†Chief, Advanced Turbomachinery Department, P.O. Box 420. Member AIAA.
‡Vice President, Research Fellow, P.O. Box 400. Associate Fellow AIAA.

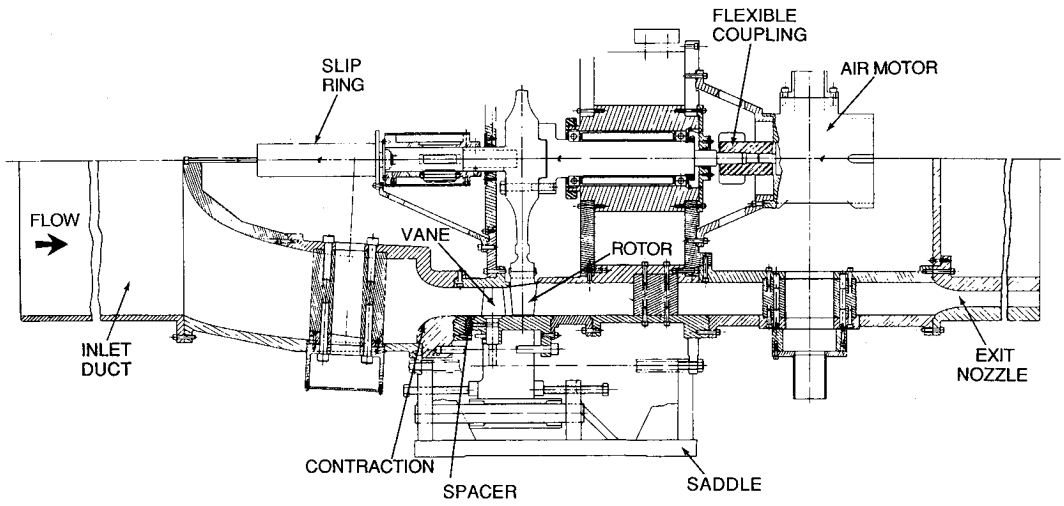

Fig. 1 Model housing turbine stage.

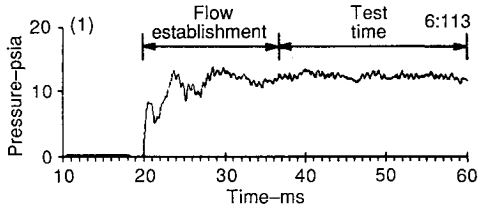

Fig. 2 Total pressure measurement time history downstream of the rotor.

bines and can be used to duplicate the flow function, Mach numbers, Reynolds numbers, corrected speed, and wall-to-gas temperature ratios associated with these engines.

The model housing the turbine stage is located in the expanding flow portion of the shock tunnel facility. Figure 1 is a sketch of the model that houses the turbine stage. The flow path consists of an inlet duct in which the Mach number is on the order of 0.05, followed by a rapid contraction in which the flow is accelerated to the vane inlet. The flow channel downstream of the rotor exit is a constant area annulus up to the exit nozzle at the rear of the model where the pressure and temperature ratios across the turbine stage are set.

The test is conducted by initially evacuating the entire facility. A fast-acting valve between the driver and driven tubes is closed and the driver tube is filled with a helium/air mixture. To start the test, the driver and driven tubes are independently pressurized to predetermined values, the rotor is brought up to speed in a vacuum, the diaphragms are broken initiating the shock wave movement down the driven tube, and a pitot probe located in the flow sends a signal to a fast-acting valve located at the end of the shock tube. This valve opens at the appropriate time, allowing test gas to enter the turbine. Total pressure time histories taken just downstream of the rotor presented in Fig. 2 show the flow establishment and test times for the system. The test time for the facility is on the order of 25 ms.

The turbine stage used in this study was designed with variable spacing between the vane and blade rows and with variable vane setting angle. Data were taken for two vane-blade spacings and two vane setting angles. The results reported herein are for the close airfoil row spacing and closed vane setting. The geometry and aerodynamic parameters for this stage are given in Tables 1 and 2, respectively. The vane exit Mach number for this case is supersonic with vane trailing-edge shocks propagating downstream into the blade row, which produces highly unsteady conditions on the blade leading edge. The inlet turbulence intensity value of 5% given in Table 2 is an estimated value based on previous measurements performed in the facility.

Table 1 VBI turbine stage geometry

	Stator	Rotor
Number of airfoils	30	45
Chord, in.	2.66	1.87
Spacing, in.	2.03	1.34
Chord/spacing	1.32	1.39
Mean radius, in.	9.73	9.70
Aspect ratio	0.72	1.10
Leading-edge radius, in.	0.18	0.09
Trailing-edge radius, in.	0.03	0.03
Hub/tip radius ratio	0.82	0.81
Tip radius, in.	10.64	10.64
Trailing-edge blockage, %	9.44	10.32

Table 2 VBI turbine stage aerodynamics

	Stator	Rotor
Rotor speed, rpm	—	11,400
Stage equivalent work, Btu/lb	—	33.7
Stage expansion ratio (total-to-static)	—	4.07
Inlet relative Mach number	0.164	0.483
Exit relative Mach number	1.121	1.054
Inlet relative flow angle, deg	0.0	−49.18
Exit relative flow angle, deg	−72.66	62.22
Inlet total temperature, °R	940	940
Inlet total pressure, psi	44.0	—
Corrected flow, lb/s	22.57	—
Inlet Reynolds number	8×10^5	—
Inlet turbulence intensity, %	5.0	—
Reduced frequency	7.8	8.5
Vane setting angle, deg	−61.0	—
Vane-blade spacing, in.	0.6	—

Time-averaged and phase-resolved pressure and heat transfer data were measured on the midspan sections of the vane and blade. The pressure data reported in this part of the article were obtained using miniature Kulite® pressure transducers. The transducers were flush mounted on the surface and had an active area of 0.025 × 0.025 in. and a thickness of 0.0139 in. A thin layer of silastic material was placed over the transducers to provide a thermal barrier. The installed frequency response of these units was in excess of 100 kHz. Figure 3 is a photograph of the vane showing the pressure transducers. The transducers were installed on the suction surface the same way as they were on the pressure surface. Care was taken to not alter the surface contour. We do not believe that the presence of the transducers influenced the results. Further details regarding the measurement/data reduction technique are given by Dunn et al.[12]

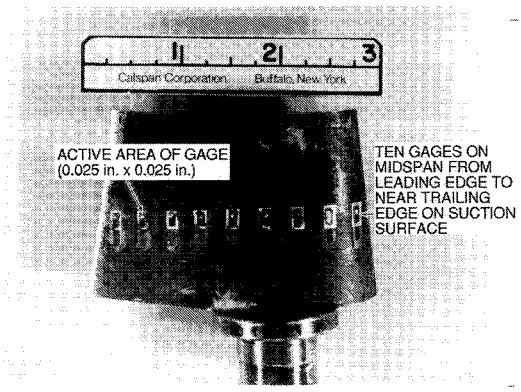

Fig. 3 Pressure gauges installed in vane.

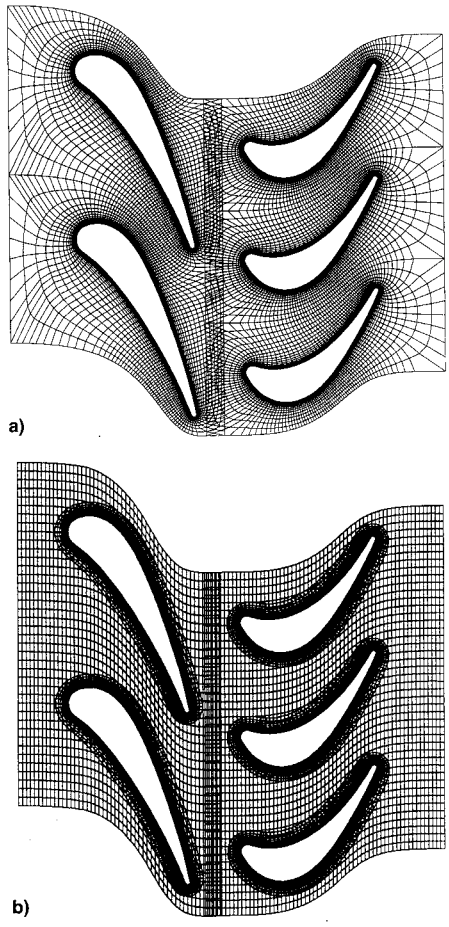

Fig. 4 Overlapping grid systems: a) capped O-grid and b) O-H grid.

Computational Method

The computational method for modeling the flow in this turbine stage is based on the implementation by Lewis et al.[11] of the phase-lagged method developed by Erdos et al.[16] to handle arbitrary airfoil counts in the two rows of a turbine stage. This method, based on overlapping O-grids, was extended by the authors[17] to a fully viscous analysis by including all of the viscous terms in the Navier-Stokes equations. Upon analyzing the results from this analysis, it has become apparent that while the surface boundary layers are adequately resolved with the system of overlapping O-grids, the grid system (shown in Fig. 4a) has a few shortcomings:

1) The O-grid used about each airfoil does not provide adequate resolution of the wake shed from the trailing edge of the upstream row because of the spreading apart of grid lines away from the airfoil surface.

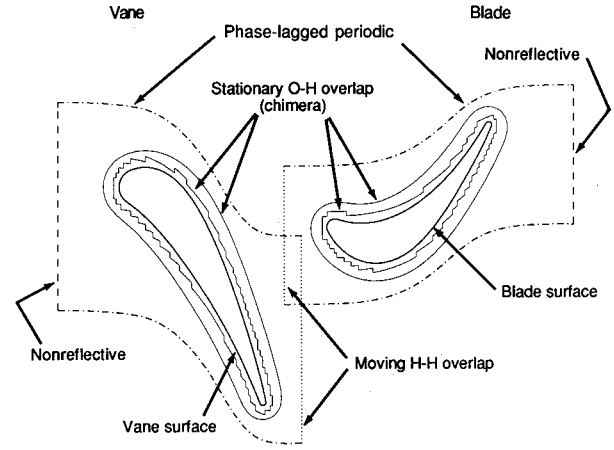

Fig. 5 Schematic of domain showing different boundary points.

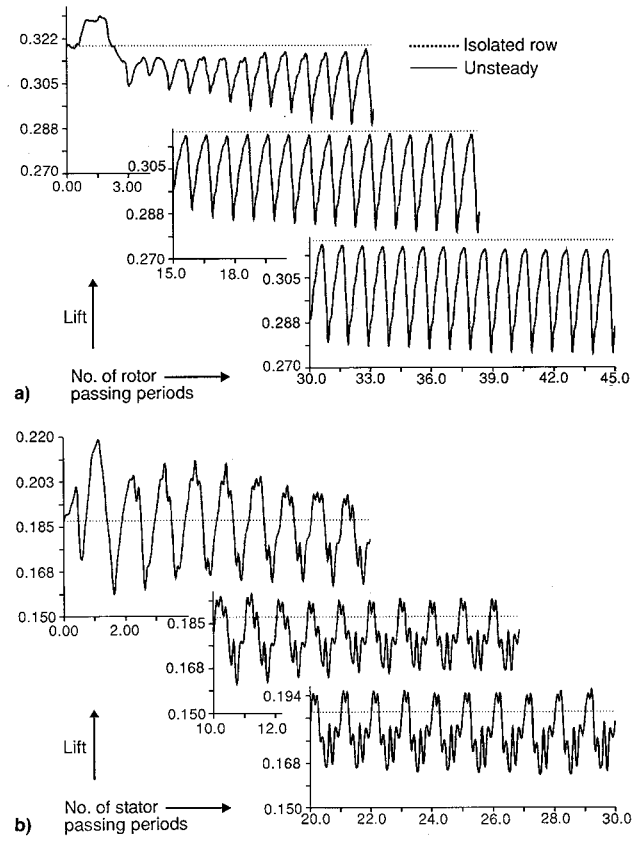

Fig. 6 Lift coefficient time histories: a) vane and b) blade.

2) It is not possible to extend the upstream and downstream boundaries of the stage computational domain far enough to employ one-dimensional inflow and outflow nonreflective boundary conditions used in the analysis without severely distorting the grid.

In order to address these limitations, an overlapping O-H grid system was implemented. The system shown in Fig. 4b incorporates airfoil conforming O-grids embedded in H-grids. The O-grids are clustered to resolve the airfoil boundary layers, and the H-grid lines are distributed to provide for adequate resolution of the wake in the interblade row region. The H-grid also provides flexibility in locating the upstream and downstream boundaries of the stage, and in positioning of the overlap interface between the blade rows.

A quasi-three-dimensional coordinate system is used for the analysis of flow on a blade-to-blade surface of revolution. Previous work by Lewis et al.[11] and the authors[17] used the explicit hopscotch finite difference scheme to solve the Euler/Navier-Stokes equations in the quasi-three-dimensional co-

Fig. 7 Instantaneous pressure contours.

ordinate system. The scheme employed a hybrid second-order artificial dissipation scheme to stabilize the solution in regions of high gradients. In this investigation an explicit five-stage Runge-Kutta time-stepping scheme presented by Swanson and Turkel[18] is used for solving the Navier-Stokes equations in the interior of the flow domain. The scheme is based on central difference approximations of the spatial derivative terms of the governing equations, and utilizes a combination of second- and fourth-order artificial dissipation. The scheme is second-order accurate in time and space. The Baldwin-Lomax model is employed to model turbulence.

Figure 5 shows the topology of the grid system and the five different types of boundary points involved in the interactive analysis. They are 1) airfoil surface boundary points on the O-grid, 2) stage inlet and exit boundary points on the H-grids, 3) boundary points along the periodic boundary of the H-grids, 4) H-H grid moving overlap boundary points, and 5) embedded grid overlap boundary points. A detailed description of the treatment of these boundary points can be found in Ref. 11, and will not be given here.

Boundary Point Calculation

At airfoil surfaces, the no slip condition is imposed. Pressure is extrapolated and the airfoil surface temperature is specified.

The stage inflow and outflow boundary point calculations were formulated to yield no reflections of outward radiating waves and were based on a reference plane method of characteristics numerical scheme originally employed by Erdos et al.[16] At the inflow boundary, the scheme solves the set of compatibility relations written in Reimann invariant form. For steady-state computations, total pressure, total temperature, and flow angle are specified at the inflow boundary, and the other variables are determined using the outgoing Riemann invariant and the isentropic flow relations. At the stage outflow boundary, two compatibility relations associated with the outgoing wave and particle path and the incoming wave are used for unsteady computations. For steady flow computations, the static pressure is fixed at the outflow boundary and the other flow variables are obtained using the outgoing particle path and the Riemann invariant relations.

Phase-lagging procedures are enforced at the grid periodic boundaries to allow for arbitrary airfoil counts in the vane and blade rows. With this procedure[11,16] the solution domain need only span one pitch in both the vane and blade rows rather than the entire circumference as is required in general by those methods enforcing spatial periodicity. The phase-lagging procedure requires the time-storage of dependent variables at points adjacent to the periodic boundaries.

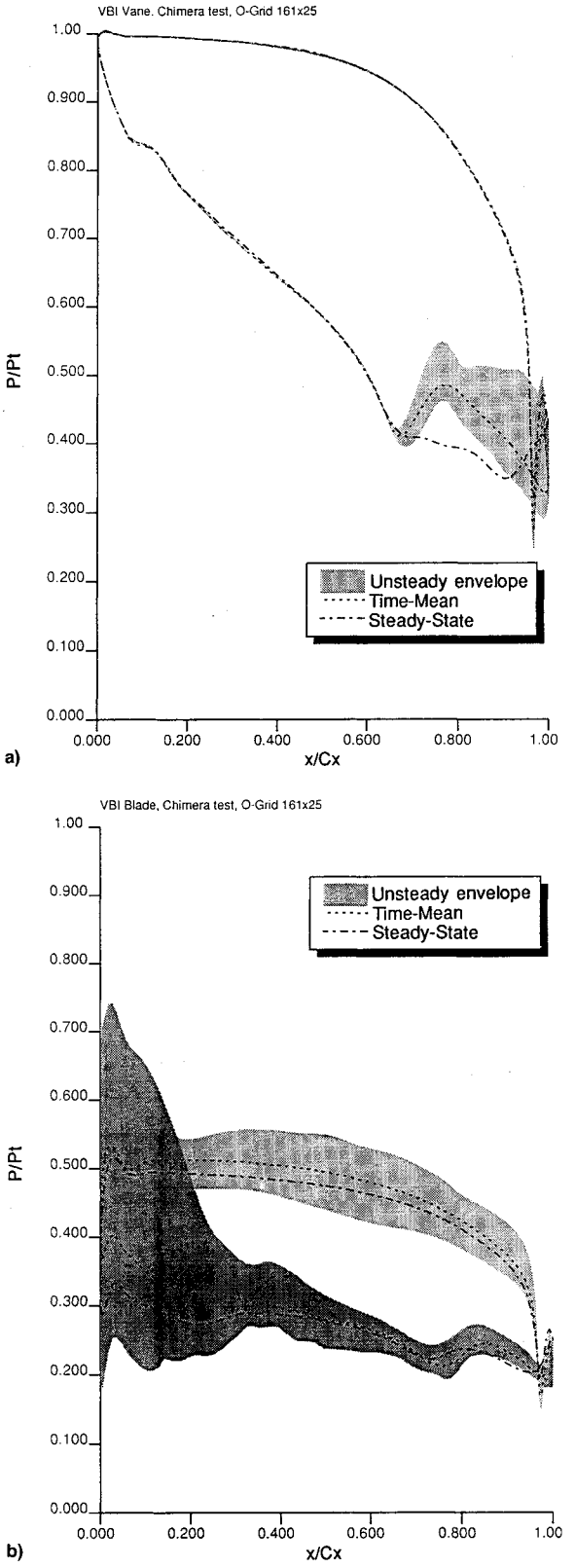

Fig. 8 Surface pressure distributions: a) vane and b) blade.

The vane and blade flowfields are coupled at the vane exit/blade inlet plane. The two grids are overlapped to enable transfer of information between the two solutions, and dependent variables at the vane exit/blade inlet are obtained by bilinear interpolation on each blade-to-blade grid surface. Since, in general, the airfoil spacing is not the same in each row, a phase-lagging procedure similar to that used at the periodic boundary is used to obtain data outside the solution domain at any particular time.

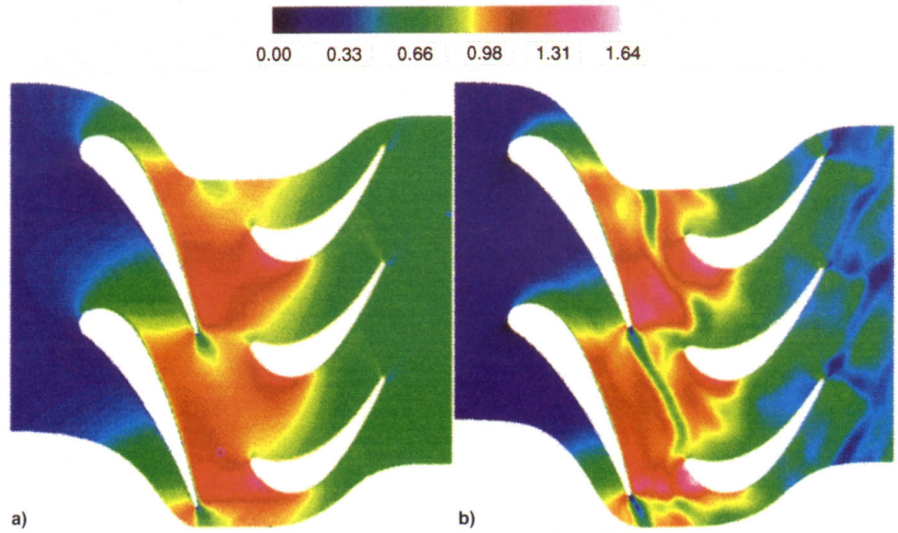

Fig. 9 Instantaneous Mach contours: a) capped O-grid and b) O-H grid.

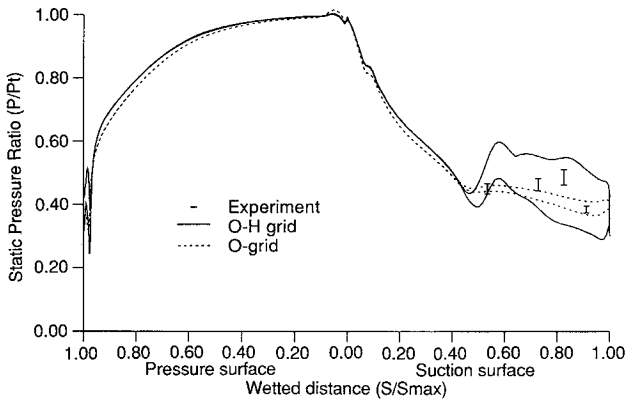

Fig. 10 Unsteady envelope of pressure on vane surface.

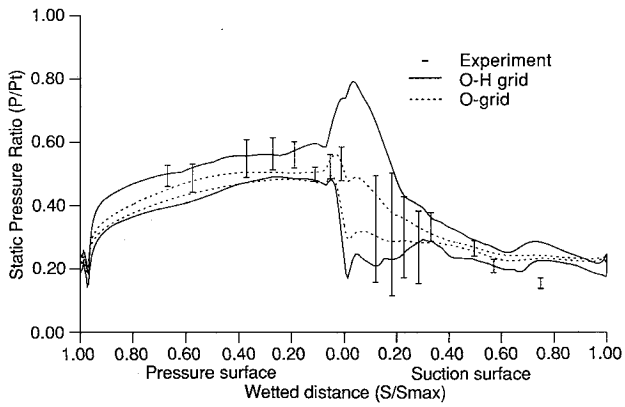

Fig. 11 Unsteady envelope of pressure on blade surface.

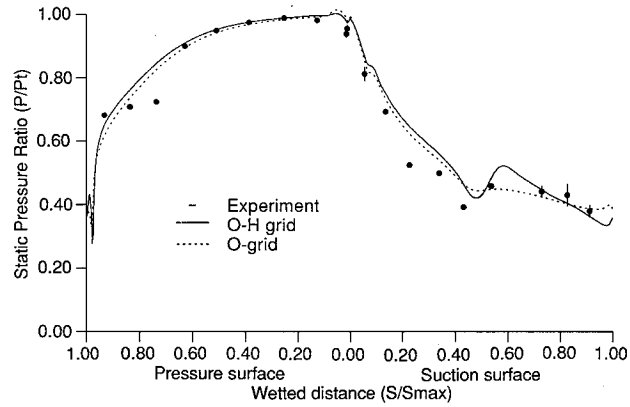

Fig. 12 Time-averaged pressure distribution on vane surface.

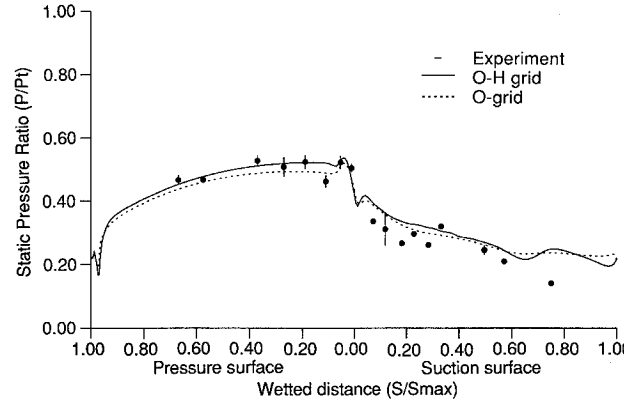

Fig. 13 Time-averaged pressure distribution on blade surface.

The chimera technique[19] is used to couple the O and H grids at the outer boundary of the O grid. This is a general purpose scheme that allows data transfer between solutions on arbitrarily overlapped grids. It is a more general scheme than that used at the vane-blade interface, and involves interpolation of data in one solution to obtain boundary condition data for the other solution.

Results

Computations for the turbine stage described previously were made on the overlapped grids shown in Fig. 4b. The unsteady interactive solution was started from steady isolated vane and blade row solutions. The steady solutions were calculated using the interactive code, but with fixed interblade-row boundary conditions prescribed at the vane exit and blade inlet, and spatially periodic conditions enforced along the grid circumferential boundaries.

The coupling between the vane and blade solutions in the interactive calculation was accomplished by interpolating inflow or outflow boundary data for the blade or vane from the other solution. Two-dimensional bilinear interpolation was used to obtain the boundary data. For unequal numbers of vanes and blades, a phase-lagging procedure was enforced along the grid circumferential boundaries instead of the spatially periodic condition.

Typically, the time required to converge the unsteady solutions was equal to the time increment for the rotor to rotate one revolution. The number of time steps for one circumfer-

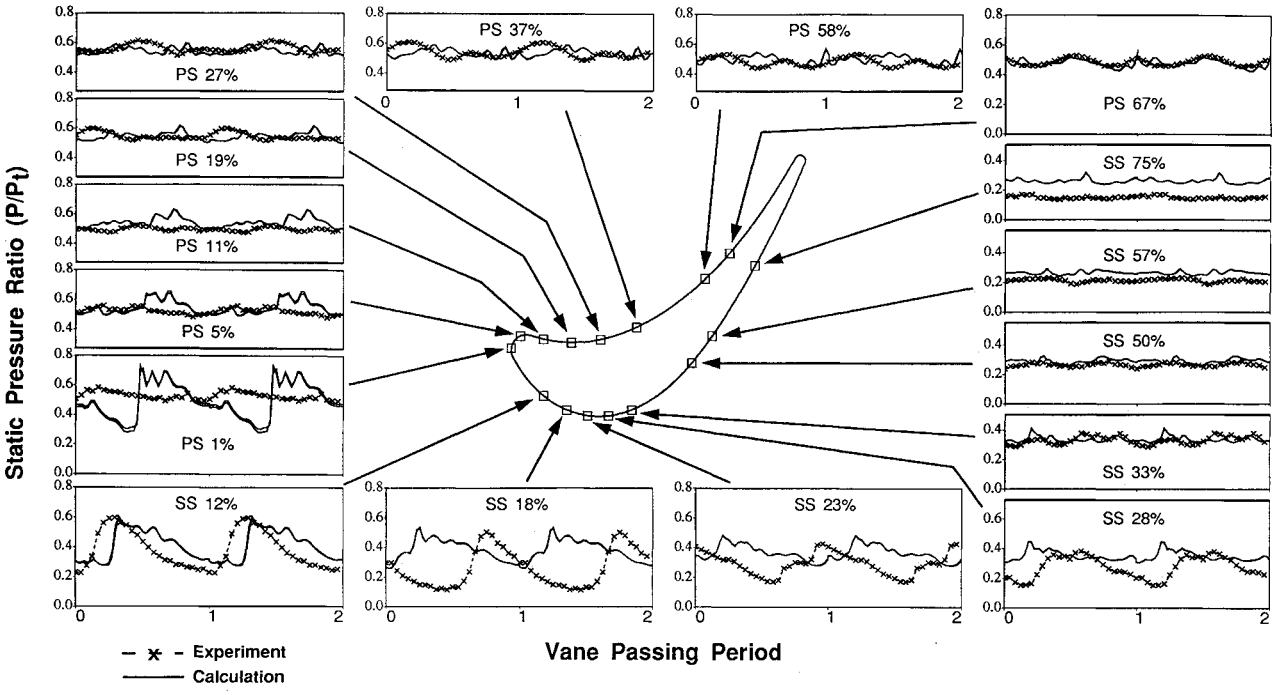

Fig. 14 Phase-resolved pressure history.

ential period (corresponding to two vane passing periods and three blade passing periods for this case) was 2580. Lift coefficient time histories for the vane and blade rows showing convergence from the steady to quasisteady solutions are presented in Fig. 6. Instantaneous pressure contours from the computations are shown in Fig. 7. The plot shows strong gradients within the vane and blade passages. Also evident are the vane trailing-edge shocks propagating downstream into the rotor. For this operating condition, the vane trailing-edge shocks impinge on the rotating blades, creating large-amplitude pressure fluctuations around the blade leading edge. The degree of unsteadiness on the airfoil surfaces is shown in Fig. 8. In this figure, the envelopes of the unsteady pressure fluctuations are presented along with the time-mean pressure distributions. The plot clearly shows that the vane row is choked with no unsteadiness propagating upstream of the throat location on the vane suction surface. The figure also shows that the blade unsteady pressure fluctuations around the airfoil leading edge are as large as the steady airfoil loading. Comparisons of the time-mean and steady-state solutions show reduced loading on the vane and lower incidence on the blade for the time-mean prediction. The difference in incidence angles on the blade is consistent with the finding of Ashworth et al.,[13] from rotating wire experiments. Ashworth attributed this apparent incidence change to the reduced velocity in the vane wakes.

Instantaneous Mach number contours from the present solution are compared with those from a capped O-grid solution obtained with the hopscotch algorithm in Fig. 9. Both plots show strong gradients within the vane and blade passages. Also evident are the vane trailing-edge shocks propagating downstream into the rotor. The wake clearly propagates further downstream with the O-H grid scheme. This is attributed to the better resolution provided by the O-H grids and to the improved dissipation model used with the numerical scheme.

Comparisons between the vane and blade envelopes of the unsteady airfoil surface pressure distributions from the O- and O-H grid scheme predictions and measurements are presented in Figs. 10 and 11, respectively, where the results are presented vs percent wetted distance along the airfoil surface. Consistent with the results in Fig. 8, no unsteadiness is predicted upstream of the vane throat in Fig. 10. Downstream of the throat on the vane suction surface, both predictions and measurements show significant unsteadiness. The unsteadiness on the vane suction surface is because of the impact of the vane trailing-edge shock reflection from the blade leading edge. The reasons for the discrepancies between the predictions are not fully understood; however, the O-H grid scheme should be more accurate than the O-grid scheme because of the higher order damping scheme employed with the Runge-Kutta algorithm. It is possible that the O-H grid solution overpredicts the unsteady excursion because it does not model the three-dimensional effects, which are thought to be important in the highly unsteady interblade row region. Modeling the flow in three dimensions would provide relief for the high gradients seen between the blade rows. The blade unsteady pressure envelopes in Fig. 11 show higher amplitude unsteadiness from the O-H grid solution than the O-grid solution, which is likely the result of better resolution with the O-H grid scheme. The O-H grid solution also shows better agreement with the data. Figure 11 clearly shows that the unsteadiness persists at a near-uniform level on the pressure surface, whereas it dies out with increasing distance from the leading edge on the suction surface. This difference is the result of the entire pressure surface being exposed to the vane trailing-edge activity, whereas the rear part of the suction surface is hidden from the vane trailing edge.

Calculated time-mean airfoil surface pressures from the O-H grid scheme are compared with measurements from the rig test[12] and with calculations from the previous capped O-grid scheme[17] in Figs. 12 and 13. These figures present the time-averaged surface pressure distributions for the vane and blade. The standard deviations over multiple tests in the experimental data are indicated by the vertical bars through the symbols. At most locations, the standard deviations fall within the symbols. On the vane pressure surface, both predictions are essentially in agreement and closely match the data, except in the vicinity of the 80% wetted distance where the data lie below the prediction. There appears to be no physical explanation from steady isolated airfoil row testing experience for the measured decrease in pressure. On the vane suction surface, the predictions are in good agreement except near 50% wetted distance where the present O-H grid solution more closely matches the data. This is attributed to the better resolution provided by the O-H scheme and the higher-order damping employed with the Runge-Kutta algorithm. The small pressure rise at 50% wetted distance indicates the presence of a weak trailing-edge shock reflection. While the O-H grid

solution predicts the presence of the shock, the shock location is not accurately predicted. The flow in this region is highly transitional and it is believed that a combination of better turbulence/transition modeling and improved grid resolution would yield predictions that more closely match the data. Figure 13 presents a comparison between the blade data and the results of the O-H grid and O-grid predictions. On both surfaces, the predictions are relatively close to each other, with the O-H grid solution matching the data more closely on the pressure surface. On the suction surface, the predictions are slightly above the data, and neither solution predicts the oscillatory behavior between 20 and 33% wetted distance. Overall, the agreement between the predictions and the measurements is good, with the O-H grid solution matching the data more closely.

Blade surface phase-resolved pressure data are compared with predictions from the O-H scheme at different locations in Fig. 14. At each gauge location, the data and predictions from the two grid points nearest to the gauge are plotted. The labels on each plot in this figure indicate the pressure surface (PS) or suction surface (SS) and the percent wetted distance from the geometric stagnation point. In Fig. 14, the beginning and end of a period is chosen arbitrarily so that the calculated phase is best matched with data for most of the gauges. However, once this reference time is chosen, it is fixed for all locations. The predicted amplitudes closely match the data. It appears that about half of the gauge pressures are out of phase relative to the predictions. On the pressure surface, the predicted and measured data agree well, whereas on the suction surface, there are some differences.

It should be noted that three-dimensional effects are only partially accounted for in the quasi-three-dimensional analysis. It is likely that the predictions will not closely match experimental data in interblade-row regions where three-dimensional effects are likely to be significant. Despite this limiting flow modeling assumption and the uncertainties with the experimental measurement accuracy, the agreement between the predictions and data is very good.

Conclusions

A two-dimensional unsteady Navier-Stokes code based on an explicit Runge-Kutta algorithm and a O-H grid system has been successfully used to predict the unsteady flow in a transonic turbine stage. The code has been shown to predict the strong interactions between the vane and blade created by the vane trailing-edge shocks impinging on the downstream rotor. Predicted time-averaged and phase-resolved airfoil surface pressure distributions show good agreement with stage data acquired in a short duration shock tunnel.

Acknowledgments

This work was funded by Air Force Contract F33615-90-C-2028. The authors wish to acknowledge J. H. Friddell of the Air Force Wright Laboratory, Ohio, for many helpful discussions. The authors would also like to thank Allison Gas Turbine Division and the U.S. Air Force for permission to publish this article.

References

[1]Hunter, I. H., "Endwall Boundary Layer Flows and Losses in an Axial Turbine Stage," *Journal of Engineering for Power*, Vol. 104, Jan. 1982, pp. 184–193.

[2]Dring, R. P., Joslyn, H. D., Hardin, L. W., and Wagner, J. H., "Research on Rotor-Stator Aerodynamic Interaction and Rotor Negative Incidence Stall," Air Force Wright Aeronautical Labs. TR-81-2114, Nov. 1981.

[3]Scholz, N., "Aerodynamics of Cascades," AGARD-AG-229, Jan. 1978.

[4]Sharma, O. P., Pickett, G. F., and Ni, R. H., "Assessment of Unsteady Flows in Turbines," *Journal of Turbomachinery*, Vol. 114, Jan. 1992, pp. 79–90.

[5]Pfeil, H., Herbst, R., and Schroder, T., "Investigation of the Laminar-Turbulent Transition of Boundary Layers Disturbed by Wakes," *Journal of Engineering for Power*, Vol. 105, Jan. 1983, pp. 130–137.

[6]Paxson, D. E., and Mayle, R. E., "Laminar Boundary Layer Interaction with an Unsteady Passing Wake," American Society of Mechanical Engineers Paper 90-GT-120, June 1990.

[7]Addison, J. S., and Hodson, H. P., "Unsteady Transition in an Axial Flow Turbine, Part 1—Measurements on the Turbine Rotor," American Society of Mechanical Engineers Paper 89-GT-289, June 1989.

[8]Addison, J. S., and Hodson, H. P., "Unsteady Transition in an Axial Flow Turbine, Part 2—Cascade Measurements and Modeling," American Society of Mechanical Engineers Paper 89-GT-290, June 1989.

[9]Doorly, D. J., and Oldfield, M. J., "Simulation of the Effects of Shock Wave Passing on a Turbine Rotor Blade," *Journal of Engineering for Gas Turbines and Power*, Vol. 107, Oct. 1985, pp. 998–1006.

[10]Giles, M. B., "Stator/Rotor Interaction in a Transonic Turbine," AIAA Paper 88-3093, July 1988.

[11]Lewis, J. P., Hall, E. J., and Delaney, R. A., "Numerical Prediction of Turbine Vane-Blade Aerodynamic Interaction," *Journal of Turbomachinery*, Vol. 111, Oct. 1989, pp. 387–393.

[12]Dunn, M. G., Bennett, W. A., Delaney, R. A., and Rao, K. V., "Investigation of Unsteady Flow Through a Transonic Turbine Stage: Data/Prediction Comparison for Time-Averaged and Phase-Resolved Pressure Data," *Journal of Turbomachinery*, Vol. 114, Jan. 1992, pp. 91–99.

[13]Ashworth, D. A., LaGraff, J. E., Schultz, D. L., and Grindrod, K. J., "Unsteady Aerodynamic and Heat Transfer Processes in a Transonic Turbine Stage," American Society of Mechanical Engineers Paper 85-GT-128, June 1985.

[14]Guenette, G. R., Epstein, A. H., Giles, M. B., Haimes, R., and Norton, R. J. G., "Fully Scaled Transonic Turbine Rotor Heat Transfer Measurements," *Journal of Turbomachinery*, Vol. 111, Jan. 1989, pp. 1–7.

[15]Rangwalla, A. A., and Madavan, N. K., "Application of an Unsteady Navier-Stokes Solver to Transonic Turbine Design," AIAA Paper 91-2468, June 1991.

[16]Erdos, J. I., Alzner, E., and McNally, W., "Numerical Solution of Periodic Transonic Flow Through a Fan Stage," *AIAA Journal*, Vol. 15, 1977, pp. 1559–1568.

[17]Rao, K. V., and Delaney, R. A., "Investigation of Unsteady Flow Through a Transonic Turbine Stage: Part I—Analysis," AIAA Paper 90-2408, July 1990.

[18]Swanson, R. C., and Turkel, E., "A Multistage Time-Stepping Scheme for the Navier-Stokes Equations," AIAA Paper 85-0035, Jan. 1985.

[19]Benek, J. A., Buning, P. G., and Steger, J. L., "A 3-D Chimera Grid Embedding Technique," AIAA Paper 85-1523, July 1985.